Phytochemistry 194 (2022) 113017

Contents lists available at ScienceDirect

Phytochemistry

journal homepage: www.elsevier.com/locate/phytochem

Monoterpene indole alkaloids from *Vinca minor* L. (Apocynaceae): Identification of new structural scaffold for treatment of Alzheimer's disease

Rudolf Vrabec [a,b], Jana Maříková [c], Miroslav Ločárek [a], Jan Korábečný [d,e], Daniela Hulcová [a,b], Anna Hošťálková [a], Jiří Kuneš [c], Jakub Chlebek [a], Tomáš Kučera [d], Martina Hrabinová [d], Daniel Jun [d], Ondřej Soukup [d,e], Vincenza Andrisano [f], Jaroslav Jenčo [a], Marcela Šafratová [b], Lucie Nováková [g], Lubomír Opletal [a], Lucie Cahlíková [a,*]

[a] *ADINACO Research Group, Department of Pharmaceutical Botany, Faculty of Pharmacy, Charles University, Heyrovskeho 1203, 500 05, Hradec Kralove, Czech Republic*
[b] *Department of Pharmacognosy, Faculty of Pharmacy, Charles University, Heyrovskeho 1203, 500 05, Hradec Kralove, Czech Republic*
[c] *Department of Bioorganic and Organic Chemistry, Faculty of Pharmacy, Charles University, Heyrovskeho 1203, 500 05, Hradec Kralove, Czech Republic*
[d] *Department of Toxicology and Military Pharmacy, Trebesska 1575, 500 05, Hradec Kralove, Czech Republic*
[e] *Biomedical Research Centre, University Hospital Hradec Kralove, Sokolska 581, 500 05, Hradec Kralove, Czech Republic*
[f] *Department for Life Quality Studies, University of Bologna, 47921, Rimini, Italy*
[g] *Department of Analytical Chemistry, Faculty of Pharmacy, Charles University, Heyrovskeho 1203, 500 05, Hradec Kralove, Czech Republic*

ARTICLE INFO

Keywords:
Vinca minor
Apocynaceae
Alzheimer's disease
Docking studies
Alkaloids
Butyrylcholinesterase
Vincaminorudeine
(−)-2-ethyl-3[2-(3-ethylpiperidinyl)-ethyl]-1*H*-indole

ABSTRACT

One undescribed indole alkaloid together with twenty-two known compounds have been isolated from aerial parts of *Vinca minor* L. (Apocynaceae). The chemical structures of the isolated alkaloids were determined by a combination of MS, HRMS, 1D, and 2D NMR techniques, and by comparison with literature data. The NMR data of several alkaloids have been revised, corrected, and missing data have been supplemented. Alkaloids isolated in sufficient quantity were screened for their *in vitro* acetylcholinesterase (AChE; E.C. 3.1.1.7) and butyrylcholinesterase (BuChE; E.C. 3.1.1.8) inhibitory activity. Selected compounds were also evaluated for prolyl oligopeptidase (POP; E.C. 3.4.21.26), and glycogen synthase 3β-kinase (GSK-3β; E.C. 2.7.11.26) inhibition potential. Significant *h*BuChE inhibition activity has been shown by (−)-2-ethyl-3[2-(3-ethylpiperidinyl)-ethyl]-1*H*-indole with an IC_{50} value of 0.65 ± 0.16 μM. This compound was further studied by enzyme kinetics, along with *in silico* techniques, to reveal the mode of inhibition. This compound is also predicted to cross the blood-brain barrier (BBB) through passive diffusion.

1. Introduction

Around 50 million people today suffer from dementia, of which Alzheimer's disease (AD) is the most common form contributing to 60–70% of all cases. According to WHO, the number of patients with dementia is expected to triple in the next 30 years. AD is a progressive, irreversible, and degenerative brain disorder, impairing cognitive abilities and memory. Its occurrence significantly rises with age; it is the 5th leading cause of death among people aged 65 and older (Alzheimer's Association, 2020; WHO, 2020). The pathogenesis of AD is still not fully understood. However, the primary triggering mechanisms are ascribed to the extracellular storage of β-amyloid (Aβ) into plaques and intracellular storage of neurofibrillary tangles (NFTs) composed of hyperphosphorylated tau protein (Blennow et al., 2006). Some Aβ species, specifically soluble oligomers, are responsible for sterile inflammation, production of free radicals, cytokines, and other neurotoxic products, which contribute to neuronal loss and atrophy of the brain (Glass et al., 2010). The pathological changes result in the deficit of the neurotransmitter acetylcholine (ACh), leading to impairment of the cholinergic neurotransmission and loss of intellectual abilities. The current

* Corresponding author. Department of Pharmaceutical Botany, Faculty of Pharmacy, Charles University, Akademika Heyrovskeho 1203, 500 05, Hradec Kralove, Czech Republic.
E-mail address: cahlikova@faf.cuni.cz (L. Cahlíková).

https://doi.org/10.1016/j.phytochem.2021.113017
Received 16 September 2021; Received in revised form 25 October 2021; Accepted 9 November 2021
Available online 16 November 2021

pharmacological treatment focuses on inhibiting the enzyme responsible for the hydrolysis of ACh, acetylcholinesterase (AChE; E.C. 3.1.1.7), thereby increasing its level in the brain and temporarily improving the symptoms of AD (Singh et al., 2013). In the later and severe stages of AD, the expression of AChE is reduced; however, another cholinesterase, specifically butyrylcholinesterase (BuChE; E.C. 3.1.1.8) production is upregulated. BuChE takes over the major role in the degradation of ACh (Douchamps and Mathis, 2017). BuChE is also involved in the production of NFTs and is associated with the formation of Aβ (Darvesh and Reid, 2016; Wright et al., 1993). Therefore, besides AChE, BuChE is considered a valid target for the treatment of AD.

Prolyl oligopeptidase (POP; E.C. 3.4.21.26) is cytosolic serine peptidase participating in the cleavage of peptides at the carboxyl end of proline. It has a regulatory function in many physiological processes since its substrates can be hormones, neuroactive peptides, and various cellular factors (Garcia-Horsman et al., 2007; Polgar, 2002). Some studies suggested the involvement of POP in the pathogenesis of AD (Hannula et al., 2013; Lambeir, 2011), thus making the inhibition of POP a potential target for AD treatment.

Glycogen synthase kinase 3β (GSK-3β; E.C. 2.7.11.26) is another enzyme involved in many physiological pathways during the cell cycle (Rayasam et al., 2009). Under pathological conditions, GSK-3β contributes to the formation of Aβ and NFTs (Maqbool et al., 2016). Compounds endowed with GSK-3β inhibition ability are well documented (Martinez et al., 2002; Naerum et al., 2002), some of which are alkaloids (Hulcova et al., 2018; Leclerc et al., 2001).

A number of AChE and BuChE inhibitors have been isolated from various natural sources. Among these natural products, alkaloids are considered the most promising candidates for use in the treatment of AD, due to their complex nitrogen-containing structures (Konrath et al., 2013). Monoterpene indole alkaloids have attracted significant interest due to their established therapeutic importance, structural diversity, and complex biosynthesis (Leonard, 1999; Zenk and Juenger, 2007). They have been extensively studied for a wide variety of pharmacological effects, such as anti-proliferative (Feng et al., 2010), anti-inflammatory (Feng et al., 2009), and AChE inhibitory activities (Cao et al., 2013).

The genus *Vinca* (Apocynaceae) comprises about six species native to Europe, northwest Africa, and southwest Asia (Koyuncu, 2012). *Vinca minor* L. is a perennial sub-shrub, indigenous to northern Spain, through western France, eastward via central and southern Europe as far as the Caucasus; it has been naturalized in many regions. In folk medicine, it is used internally for circulatory disorders, cerebral circulatory impairment, and also for supporting the metabolism of the brain. In addition, it has also been proven to enhance memory and improve several other conditions like hypertension, cystitis, gastritis, and enteritis, diarrhoea, elevated blood sugar, and to help to wean. It is used topically for sore throats, nosebleeds, bruising, abscesses, eczema, and to stop bleeding (Khanavi et al., 2010).

Vinca species are rich in indole alkaloids. *V. minor* contains mainly eburnamine-type indole alkaloids, including vincamine, which modulates brain circulation and neuronal homeostasis (Vas and Gulyas, 2005). So far, *V. minor* has been reported to contain over 50 indole alkaloids. Recently, seven such compounds have been isolated from leaves of this species which had been treated with methyl jasmonate, which causes changes in the pattern and composition of alkaloid production (Abouzeid et al., 2017). In 2012, Bahodari and colleagues reported strong anticholinesterase activity, and significant antioxidant activity of alkaloid extracts of *V. minor* and *V. major* growing in Turkey (Bahadori et al., 2012).

2. Results and discussion

2.1. Phytochemical investigation of Vinca minor

GC-MS analysis of the alkaloid extract of *V. minor* led to the initial identification of monoterpene indole alkaloids. Moreover, this extract showed interesting human cholinesterases inhibition activities ($IC_{50,h\text{-}AChE} = 191.58 \pm 38.03$ μg/mL; $IC_{50,hBuChE} = 13.60 \pm 0.82$ μg/mL). The promising bioactivities of the indole alkaloids, together with the absence of a detailed up-to-date phytochemical report on *V. minor*, encouraged us to examine this species. Extensive chromatographic purification led to the isolation of twenty-two known and one undescribed indole alkaloids (Fig. 1). The known alkaloids were identified by comparison of their MS, ESI-HRMS, 1D and 2D NMR data with the literature as vincaminorine (**1**) (Farahanikia et al., 2011; Tan et al., 2016), eburnamonine (**3**) (Kovacik and Kompiš, 1969; Li et al., 2019), minovine (**4**) (Farahanikia et al., 2011; Tan et al., 2016), vincatine (**6**, diastereoisomers 3:2) (Ali et al., 1982; Danieli et al., 1984; Döepke et al., 1969), minovincine (**7**) (Farahanikia et al., 2011; Kalaus et al., 1997; Laforteza et al., 2013; Varga et al., 2020), demethoxyalstonamide (**10**) (Ur-Rahman et al., 1991a), vincorine (**11**) (Horning and MacMillan, 2013; Mokrý et al., 1962), minovincinine (**12**) (Döepke and Meisel, 1970; Plat et al., 1962; Williams et al., 2019; Zeng et al., 2020), aspidospermidine (**13**) (Kim et al., 2017; Ma et al., 2015; Xu et al., 2019), 19-oxoeburnamonine (**14**) (Kitajima et al., 2014), akuammicine (**15**) (Hong and Vanderwal, 2017), tubotaiwine (**16**) (Martin et al., 2011), aspidofractinine (**18**) (Varga et al., 2020), 2-ethyl-3[2-(3-ethylpiperidinyl)-ethyl]-1*H*-indole (**19**) (Ur-Rahman et al., 1991b), 14, 15-dihydrovindolinine (**20**) (Yagudaev, 1984), strictamine (**21**) (Chen et al., 2018), and 5-oxoaspidofractinine (**22**) (Wenkert and Liu, 1994). The NMR data for previously described alkaloids vincaminoreine (**2**) (Farahanikia et al., 2011), 16-methoxyminovine (**5**) (Kuehne et al., 1979), 16-methoxyminovincine (**8**) (Plat et al., 1962), raucubainine (**17**) (Sierra et al., 1982), and raucubaine (**23**) (Sierra et al., 1982) have been revised, corrected and missing data added. The newly isolated alkaloid was named vincaminorudeine (**9**). Alkaloids **5**, **10**, **13**, **14**, **16**, **17**–**20**, **22**, and **23** are herein reported for the first time in this species.

Alkaloid **10** was previously isolated from *Alstonia macrophylla* Wall. ex G. Don (Ur-Rahman et al., 1991a). Alkaloid **13** was isolated from *Tabernaemontana bufalina* Lour (Shi et al., 2019). and *Rhazya stricta* Decne. (Abdel-Mogib et al., 1998), as well as alkaloid **18** and its structural types, which can be also found in *Kopsia* spp. (Kitajima et al., 2014; Wong et al., 2021). *Kopsia* spp. is also a source of alkaloid **14** (Kitajima et al., 2014). Alkaloid **16** was obtained, for example, from *T. bufalina* (Shi et al., 2019), as well as from *Haplophyton crooksii* L. D. Benson (Mroue et al., 1996). *Rauvolfia salicifolia* Griseb. is a source of alkaloids **17** and **23** (Sierra et al., 1982). Alkaloid **23** can also be found in *Alstonia costata* (G. Forst.) R. Br. (Jacquier et al., 1982). Alkaloid **20** was previously isolated from other *Vinca* spp. (Abdurakhimova et al., 1967). All of the mentioned plants belong to the Apocynacae family. So far, alkaloids **5** and **22** have not been found in a natural source, but were prepared synthetically (Kuehne et al., 1979; Wenkert and Liu, 1994). The most active alkaloid (**19**) is discussed in detail later.

The undescribed monoterpene alkaloid (**9**) exhibited a molecular ion peak $[M+H]^+$ at *m/z* 371.2339, matching the formula $C_{22}H_{30}N_2O_3^+$ (calc. 371.2329). The compound was isolated as light brown crystals, but, unfortunately, not in sufficient quantity for X-ray diffraction analysis. Moreover, none of the circular dichroism data for compounds with the required similarity were available.

However, the chemical constitution of **9** was elucidated by NMR analysis. The ^{1}H NMR spectrum revealed four signals of aromatic protons with a characteristic splitting pattern for a 1,2-disubstituted benzene ring (δ_H 7.53, dd, $J = 7.8$ Hz, $J = 1.1$ Hz, H-14; 7.27, dd, $J = 7.8$ Hz, $J = 1.1$ Hz, H-17; 7.19, td, $J = 7.8$ Hz, $J = 1.1$ Hz, H-16; 7.09, td, $J = 7.8$ Hz, $J = 1.1$ Hz, H-15), and one methine α-proton (δ_H 4.39, dd, $J = 4.3$ Hz, $J = 2.7$ Hz, H-3), the chemical shift of which was crucial for determining the relative configuration of this stereocenter (see Table 1, Fig. 2, respectively). A deshielded singlet (δ_H 3.72, s, 3-$COOCH_3$) was also observed, corresponding to a methyl ester group overlapped with a multiplet of a one proton diastereotopic methylene group (δ_H 3.75–3.70, m, H-19), as well as characteristic signals of the 1-hydroxyethyl group (δ_H 3.47, q, $J = 6.5$ Hz, H-20; 1.29, d, overlap, $J = 6.5$ Hz, H-21). The

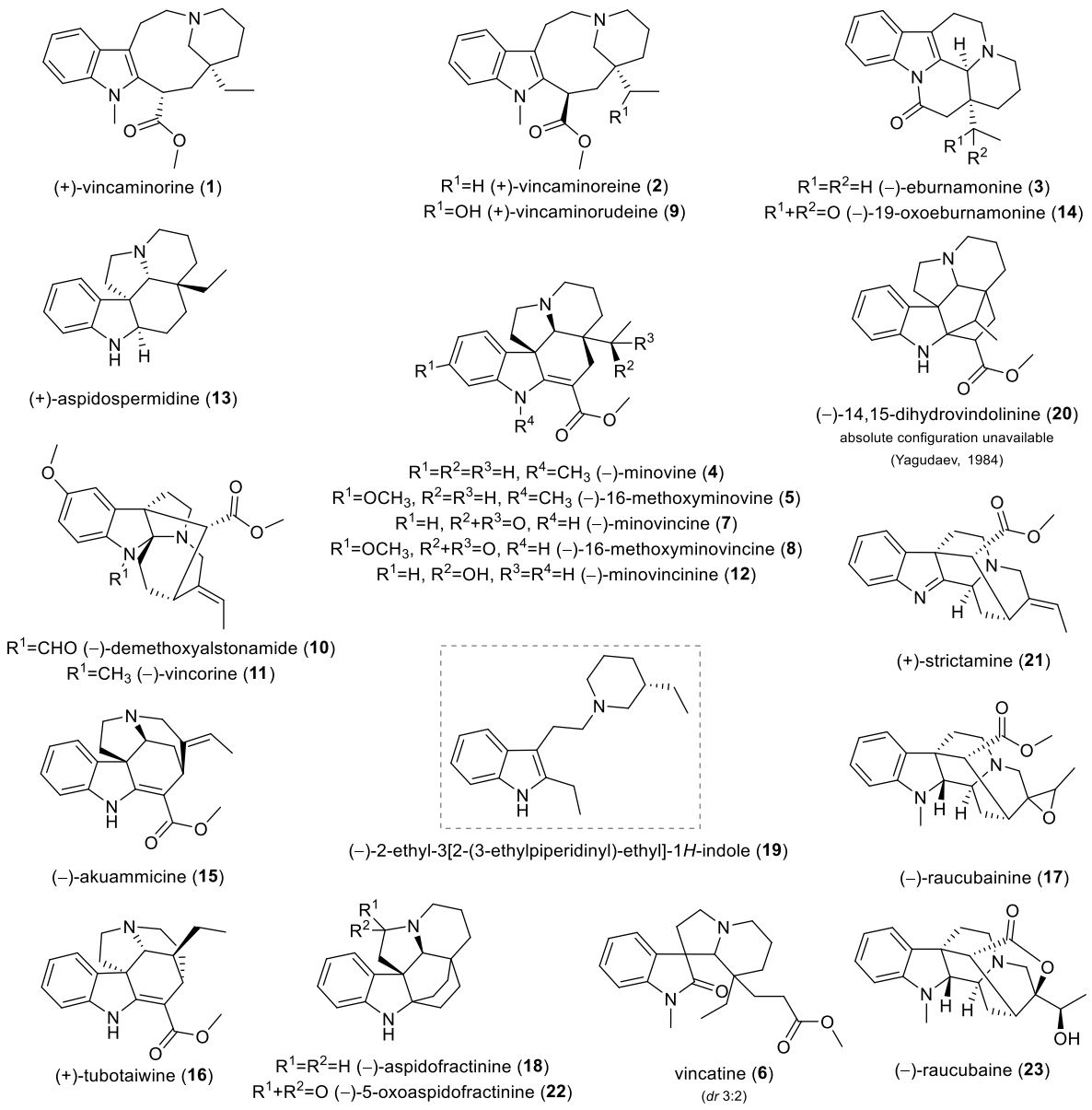

Fig. 1. Chemical structures of isolated alkaloids from aerial parts of *Vinca minor*.

signal of this methyl group overlapped with a multiplet of two protons (δ_H 1.36–1.21, m, overlap, H-7, H-6). Resonances of another eight protons were further recognized. In the ^{13}C NMR spectrum, 21 carbon signals were observed: specific chemical shifts for a methyl ester group (δ_C 177.0 and 52.7, 3-$COOCH_3$), four quaternary sp^2-carbons (δ_C 139.1, C-2; 136.7, C-18; 127.0, C-13; 110.3, C-12), four protonated sp^2-carbons (δ_C 120.7, C-16; 118.5, C-15; 118.1, C-14; 108.6, C-17), a deshielded *O*-methine group (δ_C 74.2, C-20), three *N*-methylene groups (δ_C 56.6, C-19; 55.2, C-8; 53.6, C-10), one quaternary sp^3-carbon (δ_C 42.9, C-5), one α-carbon (δ_C 38.7, C-3), four methylene groups (δ_C 31.7, C-6; 31.1, C-4; 22.3, C-11; 22.3, C-7), one *N*-methyl (δ_C 30.3, 1-CH_3), and one more shielded methyl (δ_C 17.6, C-21). Every individual signal of the proton and carbon NMR spectra was unambiguously assigned to specific groups employing HSQC experiment. Coupled spin systems were identified by correlations in the COSY and H2BC spectra, and then the *N*-methylindole moiety and hexahydroazonine cycle were established according to correlations found in the HMBC spectrum. This 9-membered ring condensed with indole is characteristic of quebrachamine-type alkaloids. Furthermore, the propylene connection of the tertiary nitrogen and quaternary carbon C-5 was determined by two-dimensional (2D) NMR experiments. The substituent of C-5 was established by HMBC cross-peaks of H-21/C-5 and H-20/C-19. All related key correlations are depicted in Table 1. Due to several reasons, the relative configuration was determined for all three chiral centers in **9**. Unfortunately, the configuration of the hydroxy methylene C-20 must be left unspecified because of a free rotation of the 1-hydroxy ethylene and the impossibility of using NOESY experiment. Moreover, it was not possible to either derivatize or analyze the compound by X-ray, as mentioned above. At least the stereochemistry of the other two carbons was determined. Because of the many conformations of the 1-azabicyclo [6.3.1]dodec-4-ene moiety, NOESY experiment was not used for the determination of its relative configuration. By comparison of the data for an analogue (**1**), a structure confirmed by X-ray crystallographic analysis, with that of its diastereomer (**2**), the relative configuration at C-3 and C-5 was determined for **9** (Tan et al., 2016).

When comparing the chemical shifts of **9** with known analogues without a 20-hydroxy substitution, vincaminorine (**1**) and its 3-epimer vincaminoreine (**2**), to confirm further the configuration of **9**, an inconsistency was found in the published data. Farahanikia et al. (2011) presented NMR data for **1** and **2**. Both these alkaloids were also isolated

Table 1
Key correlations from 2D NMR experiments in the structure elucidation of undescribed alkaloid **9** (HMBC interaction – blue arrow; H2BC and COSY interaction – red bond) and its ^{1}H and ^{13}C NMR chemical shifts assigned to the related position in ppm with coupling constants (in parenthesis, reported in Hz)..

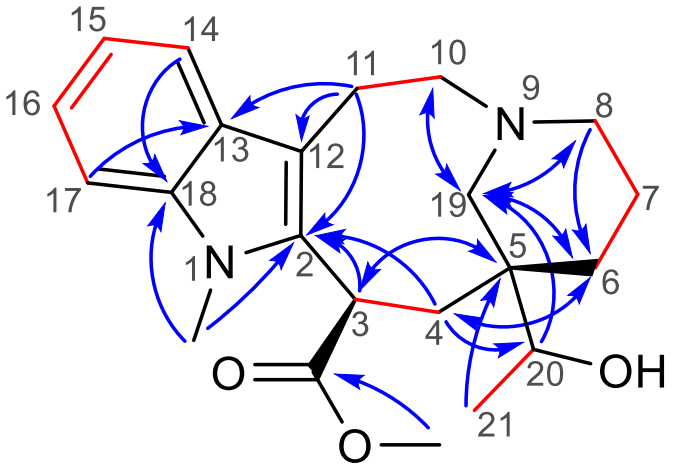

Position	vincaminorudeine 9	
	500 MHz, $CDCl_3$	125 MHz, $CDCl_3$
2		139.1
3	4.39, dd (4.1, 2.7)	38.7
4	2.63–2.55, m 1.92, dd (14.3, 4.1)	31.1
5		42.9
6	1.36–1.21, m 1.06, td (12.5, 5.5)	31.7
7	1.52–1.39, m 1.36–1.21, m	22.3
8	2.38–2.22, m	55.2
10	2.63–2.55, m 2.38–2.22, m	53.6
11	3.05–2.85, m	22.3
12		110.3
13		127.0
14	7.53, dd (7.8, 1.1)	118.1
15	7.09, dd (7.8, 1.1)	118.5
16	7.19, dd (7.8, 1.1)	120.7
17	7.27, dd (7.8, 1.1)	108.6
18		136.7
19	3.75–3.70, m, overlap 1.64, d (12.5)	56.6
20	3.47, q (6.5)	74.2
21	1.29, d, overlap (6.5)	17.6
C=O		177.0
3-$COOCH_3$	3.72, s, overlap	52.7
NCH_3	3.54, s	30.3

in our work, allowing us to compare the chemical shifts of these molecules. The interpretation of our 1D NMR spectra of **1** matched the published data of **1** prepared in the enantioselective synthesis (Tan et al., 2016). X-ray analysis confirmed the configuration of **1** in Tan's work (Tan et al., 2016). When the 3-methyl ester and 5-ethyl substituents of **1** are *cis* orientated (3*S**,5*S**), the chemical shift of the α-proton is more deshielded. The cause of this has been described in the past and is supposed to be the conformation in which this atom is centered onto *N*4 (Gilbert, 1968). Otherwise, when these substituents are in the *trans* position (3*R**,5*S**), the α-proton is more shielded, and it is found in the range of 3.90 to 3.65 ppm. Fig. 2 shows this assumption in summary for **1** and **2** supported by data of other known related 3-methyl esters. Accordingly, it was possible to elucidate the relative configuration at C-3 and C-5 of compounds **1**, **2**, and **9**.

The NMR data of **2** presented by Farahanikia et al. were different from our experimental findings (Farahanikia et al., 2011), which are summarized in Table 2. For instance, the chemical shift of α−proton (H-3) was described as a multiplet at 1.96–1.93 ppm, but our experimental data, supported by 2D NMR experiments, confirmed the resonance of H-3 at 3.90 ppm, split into a doublet of doublets ($J = 4.8$ Hz and 2.9 Hz). In Table 2, our experimental ^{1}H and ^{13}C NMR chemical shifts for **2** are compared with the previously published data. For further proof of this revision of the interpretation of the ^{1}H and ^{13}C spectra, a comparison of the chemical shifts of other 3-methyl ester quebrachamine derivatives was made (see Fig. 2).

For four isolated alkaloids, namely **5**, **8**, **17**, and **23**, relevant NMR data have not yet been published. Therefore, all compounds were extensively analysed by NMR spectroscopy (1D, and 2D NMR experiments), HRMS, polarimetry, and circular dichroism.

Compounds **5** and **8** both belong to the aspidospermine type of indole alkaloids. Compound **5** was named as (±)-*N*-methylervinceine (its synthesis was reported in 1979) (Kuehne et al., 1979), and (−)-2,3-anhydro-4-deacetoxy-6,7-dihydrovindoline, an intermediate in vindoline synthesis published in 1978 (Kutney et al., 1978). These articles provide MS, IR, UV, $[a]_D$, and melting point, but only poor interpretations of the ^{1}H NMR spectrum. Kutney et al. (1978) described the optical rotation for the synthetic intermediate as $[\alpha]_D = -377.2$ (c 0.17, $CHCl_3$). However, our experimental value was $[\alpha]_D = -21.2$ (c 0.17, $CHCl_3$). Based on these facts, data of the isolated minovine (**4**), which is a well-described alkaloid (Ishikawa et al., 2006; Tan et al., 2016; Yuan et al., 2005), were used in comparison with its 16-methoxy analog (**5**). Experimental data were correlated with those of **5** (see Table S1); accordingly, the name 16-methoxyminovine fits much more properly for structure **5** in the described context.

A similar issue occurred for **8**, with two names previously used for this compound. 16-Methoxyminovincine modified from 16-methoxyminovincinine by Oppenauer oxidation of the secondary hydroxyl, was previously described by melting point only, without analysis, but with determined stereochemistry (Döepke and Meisel, 1968). The second name used for **8** is minoriceine from the work of Zachystalová et al. (1963), which was described as an isolated indole alkaloid from *Vinca minor* L., with published analytical data for melting point, UV spectrum, and $[a]_D$. We believe that the compound presented under these names in the '60s equals **8,** the 16-methoxy derivative of the well-known *Vinca* alkaloid minovincine (**7**), also isolated in our work. According to the comparison of the 1D and 2D NMR data, and the similar optical rotation value of **8** with its analog **7** (see Table S2), the name 16-methoxyminovincine has been set for **8.**

After 2D NMR confirmation of the unusual picraline type alkaloids raucubainine (**17**) and raucubaine (**23**), only interpretations of ^{1}H NMR spectra were found in the literature as references. The identified chemical constitution of **17** with an epoxide moiety was found in the structure of raucubainine (*Rauvolfia salicifolia* Griseb., (Sierra et al., 1982)) and quaternoxine (*Alstonia quaternata* Van Heurck & Müll. Arg., (Mamatas-Kalamaras et al., 1975)), previously described diastereomers. The assignment of individual CH_3/CH_2/CH/C groups in the original article (Sierra et al., 1982) has been revised (see Table S3). Based on our analysis of the 2D NMR spectra, the interchange of methylene groups at positions 6 and 14 was recognized in comparison with the previous assignment. The red-colored bonds in Fig. 3 show COSY correlations of 3.83 (H-5)/1.69 ppm (H-6) and 3.83 (H-5)/2.72–2.68 ppm (H-6), determining the ethylene connection from the indoline moiety to the second tertiary nitrogen. In addition, the spin-spin system H-2/H-3/H-14/H-15/H-16 was also confirmed in the COSY experiment. Another proof is HMBC correlations of H-6 to the quaternary sp^2 carbon C-8, as well as correlations over three bonds of methylene H-14 to C-2, C-16, and C-20 (see Fig. 3). The results of the NOESY experiment suggest two possible orientations of the epoxide to the rest of the molecule, which was impossible to distinguish without X-ray analysis. Therefore, the configuration at C-19 and C-20 remains undetermined, as in the case with Sierra et al. (1982).

Two diastereomers, raucubaine (Sierra et al., 1982) and quaternoline

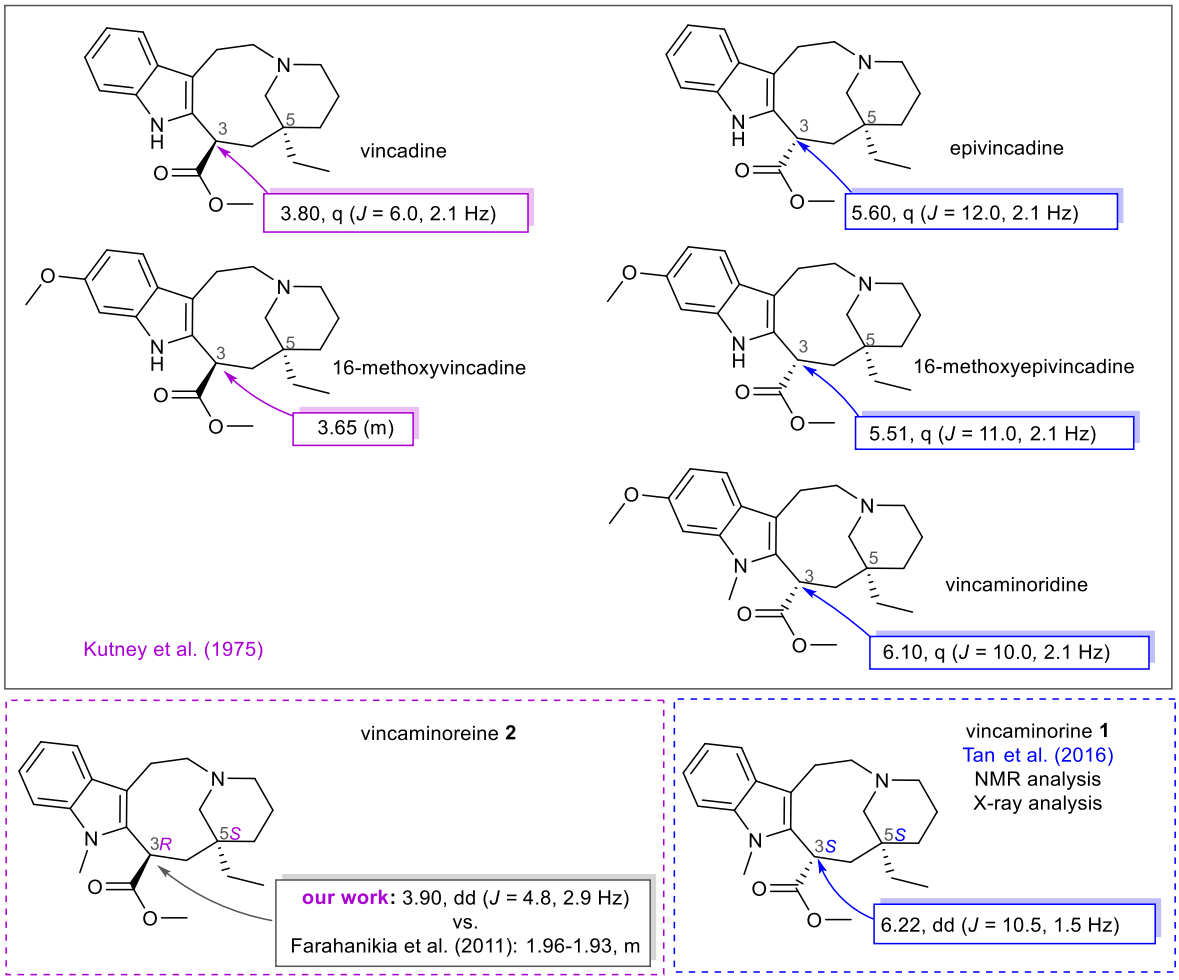

Fig. 2. Indole alkaloids with a quebrachamine framework previously described in the literature employing at least ^{1}H NMR analysis. The difference in the H-3 chemical shift of 3-epimers can be valuable for distinguishing between these diastereomers, which is highlighted. It must be mentioned that the C-3 configuration for all compounds shown was described to the contrary in Kutney's article (Kutney et al., 1975). However, the correct configuration of these alkaloids had already been identified by Kompiš et al. (1968).

(Mamatas-Kalamaras et al., 1975), are described for the constitution of **23** as well. Quaternoline was excluded from the comparison due to its poorly described analytical data, as was the case with quaternoxine and alkaloid **17**. Nevertheless, the ^{1}H NMR spectrum presented by Sierra et al. (1982) corresponds to our experimental data perfectly, along with specific optical rotation and circular dichroism data. The configuration of raucubaine was previously determined by X-ray (Pauptit and Trotter, 1981), CD analysis, and polarimetry (Sierra et al., 1982) in one collaboration. When comparing the experimental ^{1}H NMR spectral details with those published for raucubaine (Sierra et al., 1982), almost identical chemical shifts were observed (see Table S4). The missing ^{13}C NMR spectrum interpretation of **23**, with established stereochemistry of 2*R*, 3*S*,7*R*,15*R*,16*R*,19*R*,20*S*, is presented in the Supplementary Data, together with the data of other isolated known alkaloids for which the NMR spectroscopic details have not been fully reported.

2.2. Biological activity of isolated indole alkaloids

All the isolated alkaloids were tested for their inhibition of *h*AChE and *h*BuChE. Alkaloids obtained in sufficient amounts were also evaluated for their activity against POP. To determine *h*AChE and *h*BuChE inhibition properties, galanthamine and eserine were used as reference compounds. Regarding the POP inhibition assay, berberine served as a reference compound. Results of the biological studies are summarized in Table 3. In the *h*AChE assay, all isolated alkaloids were inactive (IC_{50} > 100 μM, Table 3). On the other hand, some of the alkaloids showed a promising capacity to inhibit *h*BuChE. Vincaminoreine (**2**) and vincorine (**11**) demonstrated inhibition potential in the single-digit micromolar range with IC_{50} values of = 8.71 ± 0.49 μM, and 9.75 ± 0.45 μM, respectively. The best *h*BuChE inhibition activity was demonstrated by (−)-2-ethyl-3[2-(3-ethylpiperidinyl)-ethyl]-1*H*-indole (also known as demethoxycarbonyltetrahydrosecodine (Aclinou et al., 1994), **19**) with an IC_{50} value of 650 ± 16 nM. This structurally simple indole alkaloid has been previously isolated from other Apocynaceae plants (e.g., *Haplophyton crooksii* L. D. Benson, and *Tabernaemontana pachysiphon* Stapf) and tested for its potential to inhibit AChE from electric eel (Crooks et al., 1968; Mroue et al., 1996). The obtained inhibition potency within the previous study (IC_{50} = 203 μM) is in agreement with our results (IC_{50} = > 100 μM; Table 3), pointing to very weak AChE inhibition potency. Compound (+)-**19** was isolated from the leaves of *Rhazya stricta* Decne. (Ur-Rahman et al., 1991b). The cholinesterase inhibition activity of the (+)-isomer has not been studied. Since these alkaloids are isolated from natural sources only in a limited amount, the possibility of stereoselective synthesis of the (+)-isomer was successfully explored by Palmisano et al. (1995). Both isomers can also be synthetically prepared with a shorter route by alkylation of phenylglycinol-derived bicyclic lactams (Amat et al., 2005). The preparation of semisynthetic analogues derived from **19** could be interesting for the further development of selective BuChE inhibitors.

For POP inhibition potency, alkaloid **19** was the most active

Table 2
Comparison of experimental NMR data of this work with those presented by Farahanikia et al. (2011) for the very same structure of vincaminoreine **2**. The specific optical rotation was consistent with the published one by Farahanikia et al. (2011) and Mokrý et al. (1964). ^{1}H and ^{13}C NMR chemical shifts are assigned to the related position in ppm with coupling constants for ^{1}H NMR (in parenthesis, reported in Hz)..

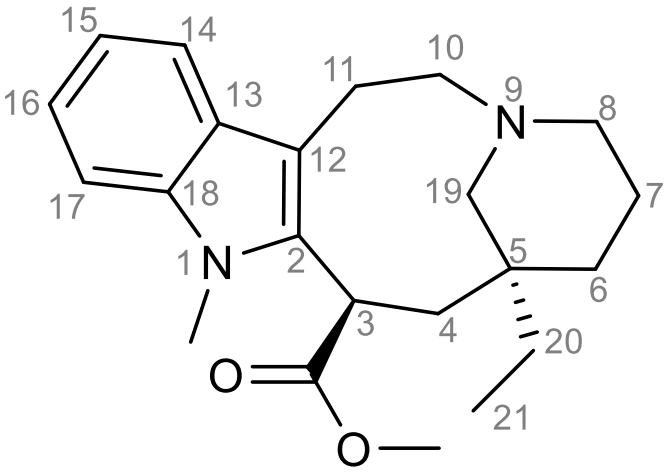

Position	Experimental vincaminoreine 2		published vincaminoreine 2 (Farahanikia et al., 2011)	
	500 MHz, $CDCl_3$	125 MHz, $CDCl_3$	500 MHz, $CDCl_3$	125 MHz, $CDCl_3$
2		139.3		139.3
3	3.90, dd (4.8, 2.9)	38.1	1.96–1.93, m	33.8
4	2.46, dd (13.7, 2.9) 1.97, d (13.7)	33.9	2.95–2.93, m	22.5
5		38.1		24.8
6	1.43–1.36, m 1.24–1.12, m	34.2	1.35–1.30, m 1.20–1.18, m	31.0
7	1.54–1.44, m 1.35–1.24, m	22.5	1.54–1.47, m 1.29–1.25, m	22.3
8	2.38–2.32, m 2.32–2.20, m	55.3	2.51–2.49, m 2.27–2.24, m	53.3
10	2.55–2.50, m 2.32–2.20, m	53.3	2.33–2.29, m 2.29–2.27, m	55.3
11	3.00–2.89, m	22.3	1.41–1.36, m 1.18–1.16, m	34.2
12		110.0		110.0
13		127.1		127.1
14	7.50, dd (7.8, 1.0)	118.0	7.50, d (7.1)	118.0
15	7.18, td (7.8, 1.0)	118.5	7.17, t (7.0)	120.6
16	7.09, td (7.8, 1.0)	120.6	7.07, t (7.0)	118.5
17	7.26, dd (7.8, 1.0)	108.6	7.24, overlap	108.6
18		136.8		136.7
19	3.16, d (12.5) 1.61, d (12.5)	57.9	3.16, d (15.0) 1.61, d (15.0)	57.9
20	1.35–1.24, m 1.24–1.12, m	31.0	1.25–1.20, m	14.2
21	0.95, t (7.5)	7.4	0.93, t (7.2)	7.4
C=O		175.2		175.2
3-$COOCH_3$	3.71, s	52.5	3.70, s	52.5
NCH_3	3.54, s	30.2	3.52, s	30.2
$[a]_D$	+27.6 (c 0.18, $CHCl_3$)		+26.5 ($CHCl_3$) (Farahanikia et al., 2011; Mokrý et al., 1964)	

compound in our study. Compound **19** revealed two-digit inhibition ability, with an IC_{50} value of 58 ± 0.45 μM (Table 3), being nearly three times more active than berberine, an isoquinoline alkaloid recognized as a POP inhibitor (Tarrago et al., 2007).

Since GSK-3β is involved in the formation of Aβ and NFTs in AD, it can be considered a promising target for developing antidementia drugs. Thus, alkaloid **19**, as the most active compound from the cholinesterase and POP inhibition assays, was also screened for its GSK-3β inhibition potency at a concentration of 100 μM. However, it showed only marginal inhibition potential (31.43 ± 3.05% inhibition of GSK-3β).

An enzyme kinetic study was carried out to explore the inhibition mechanism of active compound **19** with *h*BuChE to describe the involved interaction. Inhibition kinetics was determined from velocity curves measured at different concentrations of **19**. The type of enzyme inhibition and appropriate affinity parameter (K_i) was calculated by nonlinear regression analysis. Results for each type of model of inhibition (competitive, non-competitive, uncompetitive, and mixed) were compared by the sum-of-squares F-test. Statistical analysis showed a competitive type of inhibition ($p < 0.05$), which is in accordance with the Lineweaver–Burk (double reciprocal) plot, used for visualization of the obtained data (Fig. 4).

The intersection of lines is located on the y-axis, which means reversible competitive binding mode to the active site of the enzyme. With increasing concentration of inhibitor, the apparent V_{max} remained unchanged and K_m increased. A K_i value of 54.9 ± 8.8 nM was determined for **16** on *h*BuChE.

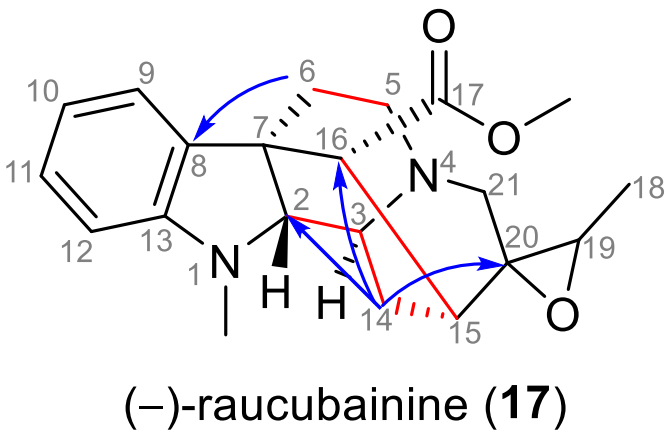

(–)-raucubainine (**17**)

Fig. 3. Described key 2D NMR correlations of revision of previously assigned positions in molecule **17** (COSY interaction – red bond, HMBC interaction – blue arrow). (For interpretation of the references to color in this figure legend, the reader is referred to the Web version of this article.)

The crucial requirement for a compound to be of clinical relevance for AD is its CNS availability; thus, the compound must penetrate through the blood-brain barrier. One of the fastest methods to predict that is the calculation of logBB, the logarithmic ratio between the concentration of a compound in the brain and blood. Compounds with logBB >0.3 have a very high probability of easy penetration by passive diffusion, whereas compounds with logBB < −1 are unlikely to pass; values between 0.3 and −1 still mean the theoretical ability for penetration (Kunwittaya et al., 2013). According to this method, all *h*BuChE active alkaloids ($IC_{50,hBuChE}$ < 10 μM) comply with this requirement (Table 3). Another commonly employed method to predict the availability of the compound to the CNS is *in vitro* parallel artificial membrane permeability assessment (PAMPA). Based on the obtained results for *in vitro* permeability of **19** ($Pe = 15.7 \pm 1.3 \times 10^{-6}$ cm s^{-1}), it can be concluded that this indole alkaloid can cross the BBB by passive diffusion (Table 3).

2.3. Docking study of (−)-2-ethyl-3[2-(3-ethylpiperidinyl)-ethyl]-1H-indole (19)

A molecular dynamic simulation was performed to determine the structural aspects crucial for the high BuChE inhibition ability of 19. The template structure of *h*BuChE was taken from Protein Data Bank (PDB ID: 4BDS) (Nachon et al., 2013). The result was compared with a crystal structure of tacrine, the first FDA-approved drug for AD therapy acting as a dual AChE/BuChE inhibitor (Soukup et al., 2013).

Molecular dynamic simulation of **19** within the *h*BuChE active site revealed several crucial interactions responsible for high ligand affinity (Fig. 5A and B). The 2-ethyl-1*H*-indole moiety of **19** is engaged in parallel π-π and displaced π-π stackings with Y440 (4.2 Å) and W430 (4.7 Å), respectively. Moreover, the 2-ethyl-1*H*-indole moiety lies in the vicinity of W82 (4.3 Å). The hydrogen atom of the indole moiety contacts the amide backbone of H438 from the catalytic triad via hydrogen bond interaction (1.9 Å). Other catalytic triad residues (S198, E325) stand aside from **19**. The protonated nitrogen atom of the 3-ethylpiperidine moiety faces towards Y332 (4.5 Å) by providing cation-π interaction. Besides, the ethyl appendage of 3-ethylpiperidine occupies the

Table 3
Biological activities of isolated *Vinca minor* alkaloids.

Compound	IC_{50} *h*AChE ± SEM (μM)[a]	IC_{50} *h*BuChE ± SEM (μM)[a]	IC_{50} POP ± SEM (μM)[a]	% inhibition of GSK-3β ± SEM[b]	logBB[c]	PAMPA (*Pe*; 10^{-6} cm s^{-1})[d]
vincaminorine (**1**)	>100	>100	429 ± 30	–	n.c.	–
vincaminoreine (**2**)	>100	8.71 ± 0.49	408 ± 60	–	−0.262	–
eburnamonine (**3**)	>100	93.49 ± 15.90	n.d.	–	n.c.	–
minovine (**4**)	>100	26.32 ± 2.52	n.d.	–	n.c.	–
16-methoxyminovine (**5**)	>100	25.01 ± 3.27	n.t.	–	n.c.	–
vincatine (**6**)	>100	43.47 ± 3.30	n.d.	–	n.c.	–
minovincine (**7**)	>100	>100	301 ± 15	–	n.c.	–
16-methoxyminovincine (**8**)	>100	>100	n.d.	–	n.c.	–
vincaminorudeine (**9**)	>100	84.91 ± 2.98	n.d.	–	n.c.	–
demethoxyalstonamide (**10**)	>100	56.38 ± 2.58	n.d.	–	n.c.	–
vincorine (**11**)	>100	9.75 ± 0.45	n.t.	–	−0.022	–
minovincinine (**12**)	>100	>100	n.d.	–	n.c.	–
aspidospermidine (**13**)	>100	33.60 ± 1.52	n.d.	–	n.c.	–
19-oxoeburnamonine (**14**)	>100	>100	n.t.	–	n.c.	–
akuammicine (**15**)	>100	38.17 ± 0.84	n.t.	–	n.c.	–
tubotaiwine (**16**)	>100	11.70 ± 0.11	n.d.	–	n.c.	–
raucubainine (**17**)	>100	93.96 ± 6.80	>500	–	n.c.	–
aspidofractinine (**18**)	>100	>100	n.d.	–	n.c.	–
2-ethyl-3[2-(3-ethylpiperidinyl)-ethyl]-1*H*-indole (**19**)	>100	**0.650 ± 0.016**	**58 ± 4**	**31.43 ± 3.05**	**−0.164**	**15.7 ± 1.3 (CNS+)**
dihydrovindolinine (**20**)	>100	>100	n.d.	–	n.c.	–
strictamine (**21**)	>100	>100	190 ± 11	–	n.c.	–
5-oxoaspidofractinine (**22**)	>100	>100	n.t.	–	n.c.	–
raucubaine (**23**)	>100	>100	n.t.	–	n.c.	–
galanthamine[e]	1.72 ± 0.12	42 ± 1	–	–	0.047	5.1 (CNS+)[f]
eserine[e]	0.063 ± 0.005	0.13 ± 0.01	–	–	−0.177	–
berberine[e]	0.72 ± 0.11	31 ± 4	142 ± 21	–	0.420	–
chlorothiazide[e]	–	–	–	–	−0.418	1.1 ± 0.5 (CNS−)

[a] Compound concentration required to decrease enzyme activity by 50%; the values are the mean ± SEM of three independent measurements, each performed in triplicate.

[b] Measured at a concentration of 100 μM.

[c] calculated at http://www.way2drug.com/geb.

[d] CNS(+): high BBB permeation predicted with P_e (10^{-6} cm s^{-1}) > 4.0, CNS(−): low BBB permeation predicted with P_e (10^{-6} cm s^{-1}) < 2.0, CNS(±): BBB permeation uncertain with P_e (10^{-6} cm s^{-1}) from 4.0 to 2.0.

[e] Reference compound; [f]Taken from reference (Stavrakov et al., 2017); n.t. stands for not tested due to the isolation of low amount; n.d. stands for not measurable due to a problem with solubility; n.c. stands for not calculated.

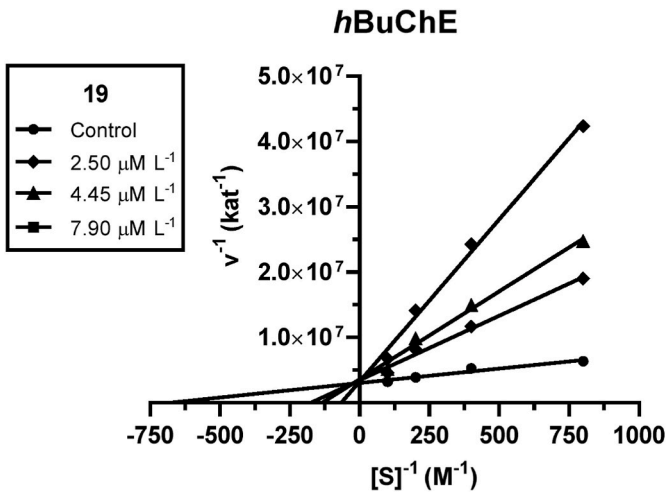

Fig. 4. Steady state competitive type inhibition of *h*BuChE substrate hydrolysis by active compound **19** at different concentrations. Lineweaver−Burk plots of initial velocity at increasing substrate concentrations (2.5–10.0 mM) are presented. Lines were derived from a linear regression of the data points. All measurements were made in triplicate and averaged.

hydrophobic region formed by F329.

Typical parallel π-π/cation-π stacking can be observed between tacrine and W82 (3.6 Å) (Fig. 5C and D) (Nachon et al., 2013). The amino group of tacrine is anchored to two water molecules, which forms a water-mediated bridge to other residues like D70, S79 and T120 (not shown). From the catalytic triad residues involved in the interaction with tacrine, hydrogen bonding between the aromatic nitrogen *N7* and the main chain carbonyl of H438 can be observed.

The overlay between **19** and tacrine is displayed in Fig. 6. Most importantly, both ligands overlap within their aromatic regions that are implicated in the π-π/cation-π stackings with W82. Similarly, both ligands contact A328, W430 and Y332 by hydrophobic interactions, albeit differently. In the case of tacrine, the aromatic part of the molecule is engaged in these interactions; for **19**, it is the 3-ethylpiperidine moiety that protrudes out to these residues. Besides the mutual amino acid residues involved in the interaction with both **19** and tacrine, **19** occupies some additional area of the *h*BuChE cavity given by the presence of the 3-ethylpiperidine moiety. This might become an area of interest for further structural changes to potentiate the inhibition ability of **19**.

3. Conclusion

In conclusion, the detailed phytochemical study of aerial parts of *V. minor* led to the isolation of twenty-two known indole monoterpene alkaloids and one undescribed structure, named vincaminorudeine (**9**). Some previously reported literature NMR data had to be revised and updated. Bioassays focused on determining the cholinesterase activity related to AD revealed that some isolated indole alkaloids are promising *h*BuChE inhibitors. The most active structure, (−)-2-ethyl-3[2-(3-ethylpiperidinyl)-ethyl]-1*H*-indole (**19**), showed remarkable *h*BuChE, and POP inhibition potency. The possibility of blood-brain barrier penetration, enzyme kinetic analysis, and binding into the active site of *h*BuChE for **19** was explored as well. The previously described synthetic routes leading to the preparation of this compound and compelling results from bioassays open an exploration possibility for its use in therapy or to classify the compound as a leading structure for the development of novel analogues.

4. Experimental

4.1. General experimental procedures

NMR spectra were recorded for $CDCl_3$ solutions at laboratory temperature on a VNMR S500 (Varian) instrument operating at 500 MHz for proton nuclei and 125.7 MHz for carbon nuclei. Chemical shifts were recorded as δ values in parts per million (ppm) and were indirectly referenced to tetramethylsilane via the solvent signal (7.26 ppm for ^1H and 77.0 ppm for ^{13}C). The coupling constant (*J*) is given in Hz, and the chemical shifts are reported in ppm. For unambiguous assignment of ^1H and ^{13}C signals, 2D NMR spectra (gCOSY, gHSQC, gHMBCAD, gH2BC, and NOESY) were obtained using standard parameter sets and pulse programs delivered by the manufacturer of the spectrometer. The MS (ESI) were measured on a Thermo Finnigan LCQDuo spectrometer. The HRMS (ESI) were obtained on a hybrid quadrupole-time-of-flight (Q-TOF) spectrometer (Waters Synapt G2Si coupled to a Waters Acquity I-Class UHPLC System). Optical rotation was measured on a P3000 polarimeter in either $CHCl_3$ or MeOH. Thin-layer chromatography (TLC) was carried out on Merck precoated silica gel F254 plates; the development solvents used were mixtures of cyclohexane (cHx), *n*-hexane (*n*-Hx), toluene (To), chloroform ($CHCl_3$), acetone (Me_2CO), diethylamine (Et_2NH), acetonitrile (ACN), ethyl acetate (EtOAc), ethanol (EtOH), light petroleum (LPE), and trifluoroacetic acid (TFAA). All used chemicals and solvents were obtained either from Sigma Aldrich (the Czech Republic), Penta – Ing. Švec (the Cech Republic), Lach-Ner (the Czech Republic), or VWR International (France). Compounds were observed under UV light (254 and 366 nm), and alkaloids were detected by spraying with Dragendorff's reagent.

4.2. Plant material

The dried aerial parts of *Vinca minor* L. (60 kg) were purchased from the herbal dealer Megafyt s.r.o. (Vrané nad Vltavou, the Czech Republic). The botanical verification was performed by prof. L. Opletal. The voucher specimen is deposited in the Department of Pharmaceutical Botany, Faculty of Pharmacy at Hradec Králové, under code AL-350.

4.3. Extraction and isolation of alkaloids

Finely cut and dried aerial parts of *V. minor* were minced and sequentially extracted with 95% EtOH (500 g of material boiling with 3 L of EtOH for 30 min). The combined extracts were evaporated, and the dry residue was dissolved in 5% HCl. Hot distilled water was added, and the formed sediment (chlorophyll) was separated. After filtration, the extract was alkalized by an aqueous solution of NH_3 to pH 9–10. The precipitate was extracted with $CHCl_3$ (5 × 15 L). The combined $CHCl_3$ extracts were evaporated to dryness, yielding 454 g of dark brown alkaloidal residue. This residue was filtered through deactivated (by 6% of water) neutral aluminum oxide (4.5 kg), washing with $CHCl_3$ (9 L). The filtered extract was concentrated to give a dark brown residue (200 g).

This purified alkaloidal extract (200 g) was separated by column chromatography on deactivated (by 6% of water) neutral aluminum oxide (6 kg) eluted with LPE gradually enriched with $CHCl_3$ (95:5, 90:10, 87.5:12.5, 85:15, 80:20, 75:25, 70:30, 65:35, 60:40, 55:45, 50:50, 45:55, 40:60, 30:70, 15:85), then with $CHCl_3$ gradually enriched with EtOH (98:2, 98:4, 94:6, 92:8, 88:12, 80:20, 70:30, 60:40). In the end, the column was washed with pure EtOH. Each fraction was collected in 500 mL portions and was monitored by analytical TLC. Overall, over 500 fractions were collected; those with similar compositions were pooled together and evaporated to dryness, yielding 19 main fractions with an overall weight of 142 g. Based on TLC and GC-MS analysis, fraction No. 8 (27 g) appeared to be qualitatively and quantitatively the richest for alkaloids. Therefore, this fraction was chosen to be further processed and investigated.

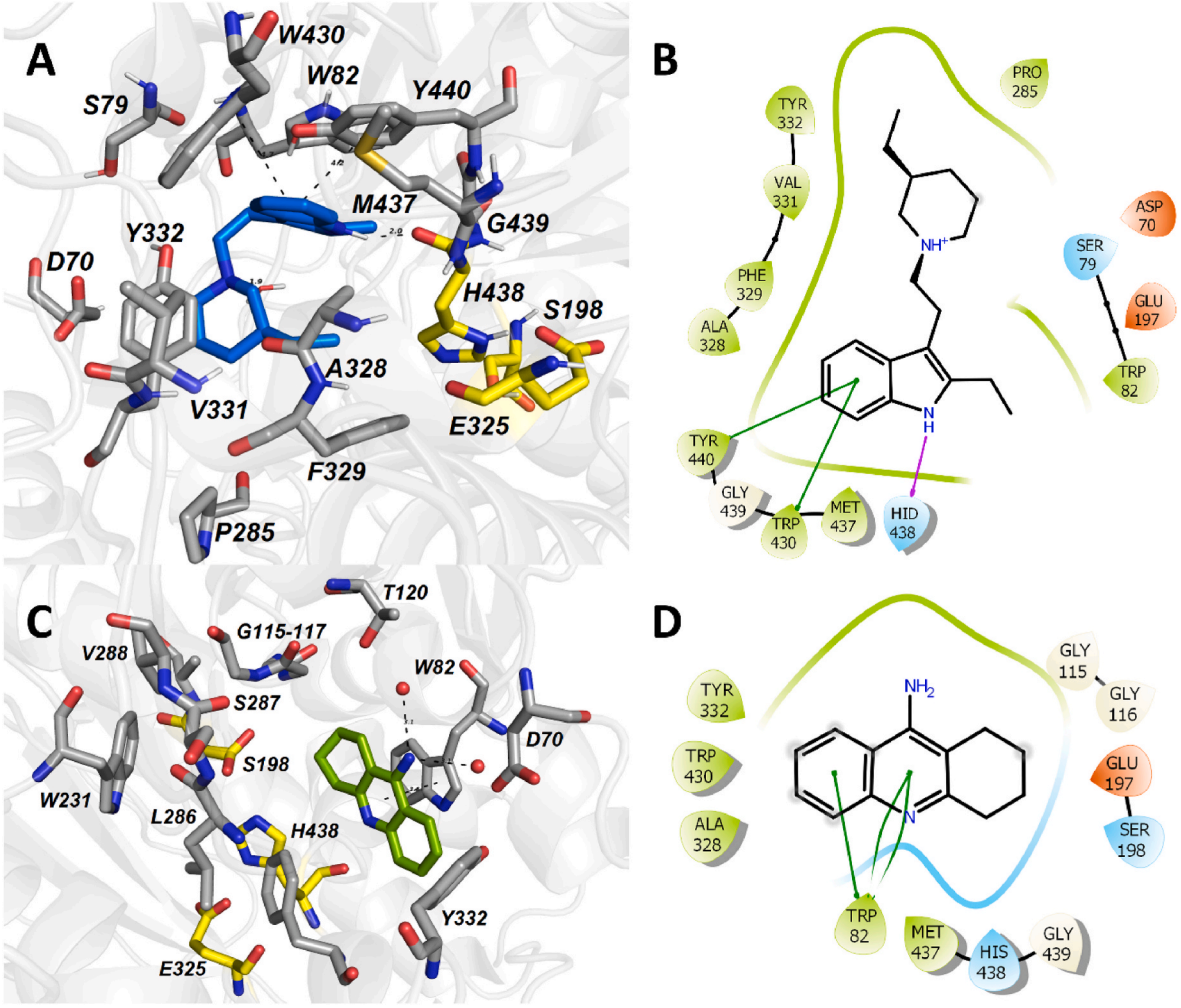

Fig. 5. The top-scored docking poses of **19** in *h*BuChE (A, B; PDB ID: 4BDS) and the crystal structure of tacrine bound to *h*BuChE (C, D). The ligands are displayed in blue (A) and green (C) for **19** and tacrine, respectively; important amino acid residues responsible for ligand anchoring are shown in grey for *h*BuChE (A, C). Catalytic triad residues are displayed in yellow (A, C). Important interactions are rendered by black dashed lines; distances are measured in angstroms (Å). The rest of the receptor is displayed in light-grey cartoon conformation (A, C). Figures A and C were created with The PyMOL Molecular Graphics System, Version 2.4.1, Schrödinger, LLC. 2D figures (B, D) were generated with Maestro 12.3 (Schrödinger Release, Schrödinger, LLC, New York, NY, 2020). (For interpretation of the references to color in this figure legend, the reader is referred to the Web version of this article.)

In the pursuit of isolation of pure alkaloidal compounds, fraction No. 8 was fractionated by column chromatography on deactivated (by 10% of water) silica gel (1.5 kg), eluting firstly with a mixture of $CHCl_3$ and LPE (80:20), then with pure $CHCl_3$, and after that with $CHCl_3$ gradually enriched with EtOH (99:1, 98:2, 95:5, 90:10). The fractions were collected in 500 mL portions and monitored by analytical TLC sprayed with Dragendorff's reagent. Overall, over 100 fractions were collected; those with similar alkaloidal TLC profiles were pooled together and evaporated to dryness, providing 8 main alkaloid-rich fractions (**A–H**).

Fraction **A** (0.59 g) was separated by preparative TLC (To–EtOAc–Et_2NH, 40:15:1, × 2) to yield vincaminorine (**1**, 54.4 mg), recrystallized from a solution of $CHCl_3$–EtOH 1:1, and vincaminoreine (**2**, 25.8 mg).

Fraction **B** (11.82 g) was dissolved in 5% HCl (pH 1) and filtered through Celite. The acidic solution of chlorides was extracted with Et_2O (4 × 50 mL) and evaporated. The residue was alkalized with 10% Na_2CO_3 (pH 9–10), and the white precipitate was extracted with Et_2O (5 × 50 mL) and evaporated once again. The alkaloidal residue was filtered and washed with distilled water, yielding 5.21 g of ocher powder. Recrystallization from a mixture of EtOH and water 1:1 yielded eburnamonine (**3**, 37.5 mg).

Fraction **C** (1.36 g) was treated by preparative TLC (*n*-Hx–EtOAc–Et_2NH, 30:11:1, × 2) to give six alkaloidal subfractions (**C1–C6**). Subfraction **C1** was purified multiple times by preparative TLC in various mobile phases (mixtures of $CHCl_3$, EtOAc, ACN, and TFAA) to finally yield minovine (**4**, 12.6 mg). Subfraction **C2** was joined with subfraction **G1** and purified by preparative TLC to give 16-methoxyminovine (**5**, 27.3 mg). TLC separation of subfraction **C3** in various mobile phases (mixtures of cHx, LPE, and Et_2NH) led to the isolation of a diastereoisomeric mixture 3:2 of vincatine (**6**, 98.1 mg). Subfraction **C4**, after treatment by preparative TLC (cHx–Et_2NH, 95:5, × 2) and purification ($CHCl_3$–ACN–TFAA, 40:10:0.1, × 1), afforded minovincine (**7**, 44.4 mg). Subfraction **C5** was separated by preparative TLC ($CHCl_3$–ACN–TFAA, 40:10:0.1, × 1) to yield 16-methoxyminovincine (**8**, 128.2 mg) and another compound, which after TLC purification (cHx–To–Et_2NH, 65:30:5, × 2), afforded the undescribed alkaloid vincaminorudeine (**9**, 18.8 mg). Finally, subfraction **C6**, after treatment by preparative TLC (cHx–Et_2NH, 95:5, × 2), yielded demethoxyalstonamide (**10**, 19.7 mg).

Preparative TLC (cHx–Et_2NH, 95:5, × 2) was used to separate fraction **D** (3.13 g) into four alkaloidal subfractions (**D1–D4**). Subfraction **D1**, after purification by preparative TLC in various mobile phases (mixtures of $CHCl_3$, ACN, TFAA, cHx, To, and Et_2NH), yielded vincorine (**11**, 33.9 mg). Subfraction **D2** contained eburnamonine (**3**, 9.8 mg).

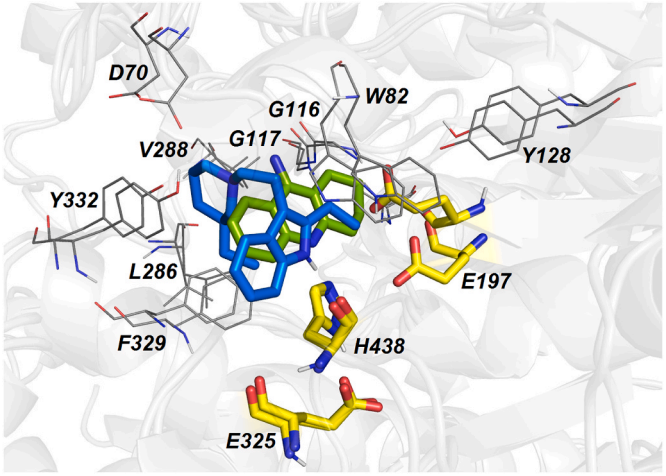

Fig. 6. Overlapped top-scored poses for ligands **19** (blue) and crystal structure of tacrine (green) in the active site of *h*BuChE (PDB ID: 4BDS). Amino acid residues involved in the interactions with ligands are depicted as either grey or yellow (catalytic triad) lines. The rest of the receptor is displayed in light-grey cartoon conformation. The Figure was created with The PyMOL Molecular Graphics System, Version 2.4.1, Schrödinger, LLC. (For interpretation of the references to color in this figure legend, the reader is referred to the Web version of this article.)

Subfraction **D3**, after further preparative TLC (cHx–EtOAc–Et_2NH, 70:30:1, × 1), gave vincaminorudeine (**9**, 26.0 mg) and a mixture of two alkaloids, which after TLC separation ($CHCl_3$–ACN–TFAA, 40:10:0.1, × 1) yielded 16-methoxyminovincine (**8**, 24.4 mg) and demethoxyalstonamide (**10**, 8.2 mg). Subfraction **D4** was entirely composed of minovincinine (**12**, 499.4 mg).

Fraction **E** (1.02 g) was subjected to preparative TLC (*n*-Hx–EtOAc–Et_2NH, 30:11:1, × 2) to give three subfractions (**E1–E3**). Subfraction **E1** was purified by TLC (cHx–LPE–Et_2NH, 80:20:4, × 3) to obtain aspidospermidine (**13**, 36.8 mg). Subfraction **E2**, merged with subfraction **G3**, was purified by repetitive TLC (To–Et_2NH, 95:5, × 1; and To–Et_2NH, 95:5, × 1) to afford 19-oxoeburnamonine (**14**, 10.0 mg). Separation of subfraction **E3** (joined together with subfraction **H3**) by preparative TLC ($CHCl_3$–ACN–TFAA, 40:10: 0.1, × 5) provided two alkaloidal zones, which after purification by further preparative TLC (*n*-Hx–To–Et_2NH, 45:45:10, × 2; and To–$CHCl_3$–Et_2NH, 70:25:5, × 2) afforded akuammicine (**15**, 8.9 mg) and tubotaiwine (**16**, 27.4 mg).

Fraction **F** (0.87 g), treated by repetitive preparative TLC (*n*-Hx–EtOAc–Et_2NH, 30:11:1, × 2), yielded raucubainine (**17**, 26.5 mg), which was recrystallized from EtOH.

Fraction **G** (0.41 g) was separated by preparative TLC to give three alkaloidal subfractions (**G1–G3**). Subfraction **G1** was joined with subfraction **C2**. Purification of subfraction **G2** by TLC (To–EtOAc–Et_2NH, 40:15:1, × 1) led to the acquisition of minovincine (**7**, 40.3 mg). Subfraction **G3** was pooled together with subfraction **E1**.

Fraction **H** (2.38 g), after treatment by preparative TLC (*n*-Hx: To–EtOAc–Et_2NH, 20:10:11:1, × 3), afforded five main subfractions (**H1–H5**). Subfraction **H1** was divided by preparative TLC (cHx–Et_2NH, 95:5, × 2) into two alkaloidal zones, which after purification by TLC (EtOAc–ACN–TFAA, 40:10:0.1, × 3; and *n*-Hx–EtOAc–Et_2NH, 30:11:1, × 2) led to the isolation of aspidofractinine (**18**, 37.1 mg) and (−)-2-ethyl-3[2-(3-ethylpiperidinyl)-ethyl]-1*H*-indole (**19**, 27.5 mg). From subfraction **H2**, treated by multiple preparative TLC (cHx–Et_2NH, 95:5, × 3; and cHx–LPE–Et_2NH, 80:20:4, × 3), 14,15-dihydrovindolinine (**20**, 65.6 mg) was obtained. Subfraction **H3** was eventually merged with subfraction **E3**. Subfraction **H4** was separated by preparative TLC (*n*-Hx–Et_2NH, 90:10, × 3) into strictamine (**21**, 89.3 mg) and another alkaloidal zone, which after purification by TLC ($CHCl_3$–ACN–TFAA, 40:10: 0.1, × 1) yielded 5-oxoaspidofractinine (**22**, 3.8 mg). Purification of subfraction **H5** by TLC (EtOAc–MeOH–Et_2NH, 40:10:2, × 1) achieved the isolation of raucubaine (**23**, 12.4 mg).

4.3.1. Vincaminorudeine (9)

Lightly brown crystals; $[\alpha]_D^{27}$ + 27.8 (c 0.1, $CHCl_3$); for ^1H and ^{13}C NMR data see Table 1; HRMS *m/z* 371.2339 $[M+H]^+$ (calc. for $C_{22}H_{30}N_2O_3^+$, 371.2329); for HRMS and 1D and 2D NMR spectra see the Supplementary Data.

4.4. Biological assays

4.4.1. Inhibition of hAChE, hBuChE

The activity of isolated alkaloids for the inhibition of human cholinesterases was assessed using the modified version of Ellman's method (Ellman et al., 1961), described recently (Al Mamun et al., 2020). The detailed description of the assay can be found in the Supplementary Data.

4.4.2. Kinetic study of hBuChE inhibition

The pharmacokinetic study of the most active substance was evaluated with the same procedure as described recently (Hostalkova et al., 2019). The details can be found in the Supplementary Data.

4.4.3. Inhibition of POP

For this assay, the same method was used as previously described (Al Mamun et al., 2020). The detailed protocol can be found in the Supplementary Data.

4.4.4. Inhibition of GSK-3β

The method for this biological test was performed according to the earlier study (Hulcova et al., 2018). Details of the procedure can be found in the Supplementary Data.

4.4.5. CNS penetration: In vitro parallel artificial membrane permeability assay (PAMPA)-blood brain barrier (BBB)

The same procedure was used as in our previous report (Cahlikova et al., 2015; Panek et al., 2017). Details of the study are available in the Supplementary Data.

4.5. Docking study

Molecular docking was used for binding poses calculations. The 3D structure ligands were built by OpenBabel, v. 2.3.2 (O'Boyle et al., 2011) and optimized by Avogadro, v. 1.2.0 using the force fields GAFF (Hanwell et al., 2012). They were converted into pdbqt-format by OpenBabel, v. 2.3.2. The *h*BuChE structure was gained from the RCSB database (PDB ID: 4BDS, resolution 2.10 Å) and prepared for docking by the function DockPrep of the software Chimera, v. 1.14 (Pettersen et al., 2004) and by MGLTools, v. 1.5.4 (Morris et al., 2009). The docking calculation was made by Vina, v. 1.1.2 as semi-flexible with flexible ligand and rigid receptor (Trott and Olson, 2010).

The docking pose of **19** was improved by MD simulation. The receptor structure was prepared using the software Chimera. The best-scored docking pose was taken as the initial for MD. The force-field parameters for ligands were assessed by Antechamber (Wang et al., 2006), v. 20.0 using General Amber force-field 2 (Wang et al., 2004). MD simulation was carried out by Gromacs, v. 2018.1 (Abraham et al., 2015). The complex receptor-ligand was solvated in the periodic water box using the TIP3P model (Mark and Nilsson, 2001). The system was neutralized by adding Na^+ and Cl^- ions to a concentration of 10 nM. The system energy was minimalized and equilibrated in a 100-ps isothermal-isochoric NVT and then a 100-ps isothermal-isobaric NPT phase. Then, a 10-ns MD simulation was run at a temperature of 300 K. The molecular docking and MD results were 3D visualized by the PyMOL Molecular Graphics System, Version 2.4.1, Schrödinger, LLC.

Declaration of competing interest

The authors declare that they have no known competing financial interests or personal relationships that could have appeared to influence the work reported in this paper.

Acknowledgment

The authors wish to thank Prof. Gerald Blunden for the critical reading of the manuscript and corrections of English. This project was supported by Charles University grants (SVV UK 260 548, Progres/UK Q42), by project "Modernization and extension of the doctoral study field of Pharmacognosy and toxicity of natural products" in the study program Pharmacy (reg. No. CZ.02.2.69/0.0/0.0/16_018/0002736), by Czech Science Foundation (project No. 20–29633J), and by Long-term development plan (Faculty of Military Health Sciences). Computational resources were provided by the CESNET LM2015042 and the CERIT Scientific Cloud LM2015085, provided under the program "Projects of Large Research, Development, and Innovations Infrastructures".

Appendix A. Supplementary data

Supplementary data to this article can be found online at https://doi.org/10.1016/j.phytochem.2021.113017.

References

Abdel-Mogib, M., Basaif, S.A., Ezmirly, S.T., 1998. Aspidospermidine and dehydroaspidospermidine from *Rhazya stricta*. J. Saudi Chem. Soc. 2, 141–143.

Abdurakhimova, N., Yuldashev, P.K., Yunusov, S.Y., 1967. The structure of majdine, pseudokopsinine, and vinervinine. Chem. Nat. Compd. 3, 263–266. https://doi.org/10.1007/BF00574630.

Abouzeid, S., Beutling, U., Surup, F., Bar, F.M.A., Amer, M.M., Badria, F.A., Yahyazadeh, M., Bronstrup, M., Selmar, D., 2017. Treatment of *Vinca minor* leaves with methyl jasmonate extensively alters the pattern and composition of indole alkaloids. J. Nat. Prod. 80, 2905–2909. https://doi.org/10.1021/acs.jnatprod.7b00424.

Abraham, M.J., Murtola, T., Schulz, R., Páll, S., Smith, J.C., Hess, B., Lindahl, E., 2015. GROMACS: high performance molecular simulations through multi-level parallelism from laptops to supercomputers. SoftwareX 1–2, 19–25. https://doi.org/10.1016/j.softx.2015.06.001.

Aclinou, P., Massiot, G., Menhour, B., 1994. Total synthesis of Crooksidine. Nat. Prod. Lett. 5, 197–200. https://doi.org/10.1080/10575639408044059.

Al Mamun, A., Marikova, J., Hulcova, D., Janousek, J., Safratova, M., Novakova, L., Kucera, T., Hrabinova, M., Kunes, J., Korabecny, J., Cahlikova, L., 2020. Amaryllidaceae alkaloids of Belladine-type from *Narcissus pseudonarcissus* cv. Carlton as new selective inhibitors of butyrylcholinesterase. Biomolecules 10, 800. https://doi.org/10.3390/biom10050800.

Ali, E., Chakraborty, P.K., Chakravarty, A.K., Pakrashi, S.C., 1982. Synthesis and stereochemistry of (±)-Vincatine. Heterocycles 19, 1667–1671. https://doi.org/10.3987/R-1982-09-1667.

Alzheimer's Association, 2020. 2020 Alzheimer's disease facts and figures. Alzheimers. Dement. 16, 391–460. https://doi.org/10.1002/alz.12068.

Amat, M., Escolano, C., Llor, N.R., Lozano, O., Gomez-Esque, A., Griera, R., Bosch, J., 2005. Alkylation of phenylglycinol-derived bicyclic lactams. Enantioselective synthesis of 3-alkylpiperidines. ARKIVOC 115–123. https://doi.org/10.3998/ark.5550190.0006.912.

Bahadori, F., Topçu, G., Boğa, M., Türkekul, A., Kolak, U., Kartal, M., 2012. Indole alkaloids from *Vinca major* and *V. minor* growing in Turkey. Nat. Prod. Commun. 7, 731–734. https://doi.org/10.1177/1934578X1200700610.

Blennow, K., de Leon, M.J., Zetterberg, H., 2006. Alzheimer's disease. Lancet 368, 387–403. https://doi.org/10.1016/s0140-6736(06)69113-7.

Cahlikova, L., Perez, D.I., Stepankova, S., Chlebek, J., Safratova, M., Hostalkova, A., Opletal, L., 2015. *In vitro* inhibitory effects of 8-O-Demethylmaritidine and Undulatine on acetylcholinesterase and their predicted penetration across the blood-brain barrier. J. Nat. Prod. 78, 1189–1192. https://doi.org/10.1021/acs.jnatprod.5b00191.

Cao, X.F., Wang, J.S., Wang, X.B., Luo, J., Wang, H.Y., Kong, L.Y., 2013. Monoterpene indole alkaloids from the stem bark of *Mitragyna diversifolia* and their acetylcholine esterase inhibitory effects. Phytochemistry 96, 389–396. https://doi.org/10.1016/j.phytochem.2013.10.002.

Chen, Z.T., Xiao, T., Tang, P., Zhang, D., Qin, Y., 2018. Total synthesis of akuammiline alkaloid (+)-strictamine. Tetrahedron 74, 1129–1134. https://doi.org/10.1016/j.tet.2018.01.034.

Crooks, P.A., Robinson, B., Smith, G.F., 1968. Isolation and structure of an indole alkaloid of biogenetic interest from *Tabernamontana cumminsii*. Chem. Commun. 1210. https://doi.org/10.1039/C19680001210, 1210.

Danieli, B., Lesma, G., Palmisano, G., Riva, R., Tollari, S., 1984. Absolute configuration of (−)-vincatine, the unique 2,16-seco Aspidosperma alkaloid. J. Org. Chem. 49, 547–551. https://doi.org/10.1021/jo00177a033.

Darvesh, S., Reid, G.A., 2016. Reduced fibrillar beta-amyloid in subcortical structures in a butyrylcholinesterase-knockout Alzheimer disease mouse model. Chem. Biol. Interact. 259, 307–312. https://doi.org/10.1016/j.cbi.2016.04.022.

Döepke, W., Meisel, H., 1968. 16-Methoxyvincadifformine, a new alkaloid from *Vinca minor*. Pharmazie 23, 521–522.

Döepke, W., Meisel, H., 1970. Stereochemistry of a new alkaloid from *Vinca minor*. Tetrahedron Lett. 11, 749–751. https://doi.org/10.1016/S0040-4039(01)97820-7.

Döepke, W., Meisel, H., Fehlhaber, H.W., 1969. Structure of vincatine, an oxindole alkaloid from *Vinca minor*. Tetrahedron Lett. 10, 1701–1704. https://doi.org/10.1016/S0040-4039(01)87985-5.

Douchamps, V., Mathis, C., 2017. A second wind for the cholinergic system in Alzheimer's therapy. Behav. Pharmacol. 28, 112–123. https://doi.org/10.1097/FBP.0000000000000300.

Ellman, G.L., Courtney, K.D., Andres, V., Featherstone, R.M., 1961. A new and rapid colorimetric determination of acetylcholinesterase activity. Biochem. Pharmacol. 7, 88–95. https://doi.org/10.1016/0006-2952(61)90145-9.

Farahanikia, B., Akbarzadeh, T., Jahangirzadeh, A., Yassa, N., Ardekani, M.R.S., Mirnezami, T., Hadjiakhoondi, A., Khanavi, M., 2011. Phytochemical investigation of *Vinca minor* cultivated in Iran. Iran. J. Pharm. Res. (IJPR) 10, 777–785. https://doi.org/10.22037/IJPR.2011.992.

Feng, T., Li, Y., Cai, X.H., Gong, X., Liu, Y.P., Zhang, R.T., Zhang, X.Y., Tan, Q.G., Luo, X.D., 2009. Monoterpenoid indole alkaloids from *Alstonia yunnanensis*. J. Nat. Prod. 72, 1836–1841. https://doi.org/10.1021/np900374s.

Feng, T., Li, Y., Liu, Y.P., Cai, X.H., Wang, Y.Y., Luo, X.D., 2010. Melotenine A, a cytotoxic monoterpenoid indole alkaloid from *Melodinus tenuicaudatus*. Org. Lett. 12, 968–971. https://doi.org/10.1021/ol1000022.

Garcia-Horsman, J.A., Mannisto, P.T., Venalainen, J.I., 2007. On the role of prolyl oligopeptidase in health and disease. Neuropeptides 41, 1–24. https://doi.org/10.1016/j.npep.2006.10.004.

Gilbert, B., 1968. Chapter 9 the alkaloids of Aspidosperma, Ochrosia, Pleiocarpa, Melodinus, and related Genera. In: Manske, R.H.F. (Ed.), The Alkaloids: Chemistry and Physiology. Academic Press, Cambridge, pp. 205–306. https://doi.org/10.1016/S1876-0813(08)60121-9.

Glass, C.K., Saijo, K., Winner, B., Marchetto, M.C., Gage, F.H., 2010. Mechanisms underlying inflammation in neurodegeneration. Cell 140, 918–934. https://doi.org/10.1016/j.cell.2010.02.016.

Hannula, M.J., Myohanen, T.T., Tenorio-Laranga, J., Mannisto, P.T., Garcia-Horsman, J. A., 2013. Prolyl oligopeptidase colocalizes with α-synuclein, β-amyloid, tau protein and astroglia in the post-mortem brain samples with Parkinson's and Alzheimer's diseases. Neuroscience 242, 140–150. https://doi.org/10.1016/j.neuroscience.2013.03.049.

Hanwell, M.D., Curtis, D.E., Lonie, D.C., Vandermeersch, T., Zurek, E., Hutchison, G.R., 2012. Avogadro: an advanced semantic chemical editor, visualization, and analysis platform. J. Cheminf. 4, 17. https://doi.org/10.1186/1758-2946-4-17.

Hong, A.Y., Vanderwal, C.D., 2017. A sequential cycloaddition strategy for the synthesis of Alsmaphorazine B traces a path through a family of Alstonia alkaloids. Tetrahedron 73, 4160–4171. https://doi.org/10.1016/j.tet.2016.11.004.

Horning, B.D., MacMillan, D.W.C., 2013. Nine-step enantioselective total synthesis of (−)-vincorine. J. Am. Chem. Soc. 135, 6442–6445. https://doi.org/10.1021/ja402933s.

Hostalkova, A., Marikova, J., Opletal, L., Korabecny, J., Hulcova, D., Kunes, J., Novakova, L., Perez, D.I., Jun, D., Kucera, T., Andrisano, V., Siatka, T., Cahlikova, L., 2019. Isoquinoline alkaloids from *Berberis vulgaris* as potential lead compounds for the treatment of Alzheimer's disease. J. Nat. Prod. 82, 239–248. https://doi.org/10.1021/acs.jnatprod.8b00592.

Hulcova, D., Breiterova, K., Siatka, T., Klimova, K., Davani, L., Safratova, M., Hostalkova, A., de Simone, A., Andrisano, V., Cahlikova, L., 2018. Amaryllidaceae alkaloids as potential glycogen synthase kinase-3β inhibitors. Molecules 23, 719. https://doi.org/10.3390/molecules23040719.

Ishikawa, H., Elliott, G.I., Velcicky, J., Choi, Y., Boger, D.L., 2006. Total synthesis of (−)- and ent-(+)-vindoline and related alkaloids. J. Am. Chem. Soc. 128, 10596–10612. https://doi.org/10.1021/ja061256t.

Jacquier, M.J., Vercauteren, J., Massiot, G., Le Men-Olivier, L., Pusset, J., Sevenet, T., 1982. Alkaloids of *Alstonia plumosa*. Phytochemistry 21, 2973–2977. https://doi.org/10.1016/0031-9422(80)85080-1.

Kalaus, G., Juhasz, I., Greiner, I., Kajtar-Peredy, M., Brlik, J., Szabo, L., Szantay, C., 1997. Synthesis of vinca alkaloids and related compounds. 90. New results in the synthesis of alkaloids with the aspidospermane skeleton. First total synthesis of (±)-3-oxominovincine. J. Org. Chem. 62 https://doi.org/10.1021/jo9713464, 9188–9191.

Khanavi, M., Pourmoslemi, S., Farahanikia, B., Hadjiakhoondi, A., Ostad, S.N., 2010. Cytotoxicity of *Vinca minor*. Pharm. Biol. 48, 96–100. https://doi.org/10.3109/13880200903046187.

Kim, J.-Y., Suhl, C.-H., Lee, J.-H., Cho, C.-G., 2017. Directed Fischer indolization as an approach to the total syntheses of (+)-Aspidospermidine and (−)-Tabersonine. Org. Lett. 19, 6168–6171. https://doi.org/10.1021/acs.orglett.7b03078.

Kitajima, M., Anbe, M., Kogure, N., Wongseripipatana, S., Takayama, H., 2014. Indole alkaloids from *Kopsia jasminiflora*. Tetrahedron 70, 9099–9106. https://doi.org/10.1016/j.tet.2014.10.002.

Kompiš, I., Mokrý, J., 1968. Alkaloids from *Vinca minor* L. XXI. Structure of vincaminoridine and vincoridine. Collect. Czech. Chem. Commun. 33, 4328–4336. https://doi.org/10.1135/cccc19684328.

Konrath, E.L., Passos, C.D., Klein, L.C., Henriques, A.T., 2013. Alkaloids as a source of potential anticholinesterase inhibitors for the treatment of Alzheimer's disease. J. Pharm. Pharmacol. 65, 1701–1725. https://doi.org/10.1111/jphp.12090.

Kovacik, V., Kompiš, I., 1969. *Vinca minor* alkaloids. XXIII. Mass spectrometry of eburnamine-type alkaloids. Collect. Czech. Chem. Commun. 34, 2809–2818. https://doi.org/10.1135/cccc19692809.

Koyuncu, M., 2012. A new species of *Vinca* (Apocynaceae) from eastern Anatolia, Turkey. Turk. J. Bot. 36, 247–251. https://doi.org/10.3906/bot-1103-19.

Kuehne, M.E., Huebner, J.A., Matsko, T.H., 1979. Studies in biomimetic alkaloid syntheses. 4. An alternative route to secodine intermediates providing syntheses of minovine, vincadifformine, ervinceine, and N(a)-methylervinceine. J. Org. Chem. 44, 2477–2480. https://doi.org/10.1021/jo01328a030.

Kunwittaya, S., Nantasenamat, C., Treeratanapiboon, L., Srisarin, A., Isarankura-Na-Ayudhya, C., Prachayasittikul, V., 2013. Influence of logBB cut-off on the prediction of blood-brain barrier permeability. Biomed. Appl. Technol. J. 1, 16–34.

Kutney, J.P., Chan, K.K., Failli, A., Fromson, J.M., Gletsos, C., Leutwiler, A., Nelson, V.R., de Souza, J.P., 1975. Total synthesis of indole and dihydroindole alkaloids. VI. The total synthesis of some monomeric vinca alkaloids: dl-vincadine, dl-vincaminoreine, dl-vincaminorine, dl-vincadifformine, dl-minovine and dl-vincaminoridine. Helv. Chim. Acta 58, 1648–1671. https://doi.org/10.1002/hlca.19750580620.

Kutney, J.P., Bunzli-Trepp, U., Chan, K.K., De Souza, J.P., Fujise, Y., Honda, T., Katsube, J., Klein, F.K., Leutwiler, A., 1978. Total synthesis of indole and dihydroindole alkaloids. 14. A total synthesis of vindoline. J. Am. Chem. Soc. 100, 4220–4224. https://doi.org/10.1021/ja00481a035.

Laforteza, B.N., Pickworth, M., MacMillan, D.W.C., 2013. Enantioselective total synthesis of (−)-minovincine in nine chemical steps: an approach to ketone activation in cascade catalysis. Angew Chem. Int. Ed. Engl. 52, 11269–11272. https://doi.org/10.1002/anie.201305171.

Lambeir, A.M., 2011. Interaction of prolyl oligopeptidase with α-synuclein. CNS Neurol. Disord. - Drug Targets 10, 349–354. https://doi.org/10.2174/187152711794653878.

Leclerc, S., Garnier, M., Hoessel, R., Marko, D., Bibb, J.A., Snyder, G.L., Greengard, P., Biernat, J., Wu, Y.Z., Mandelkow, E.M., Eisenbrand, G., Meijer, L., 2001. Indirubins inhibit glycogen synthase kinase-3 beta and CDK5/p25, two protein kinases involved in abnormal tau phosphorylation in Alzheimer's disease. A property common to most cycline-dependent kinase inhibitors? J. Biol. Chem. 276, 251–260. https://doi.org/10.1074/jbc.M002466200.

Leonard, J., 1999. Recent progress in the chemistry of monoterpenoid indole alkaloids derived from secologanin. Nat. Prod. Rep. 16, 319–338. https://doi.org/10.1039/a707500f.

Li, G., Piemontesi, C., Wang, Q., Zhu, J.P., 2019. Stereoselective total synthesis of Eburnane-type Alkaloids enabled by conformation-directed cyclization and rearrangement. Angew Chem. Int. Ed. Engl. 58, 2870–2874. https://doi.org/10.1002/anie.201813920.

Ma, H.C., Xie, X.G., Jing, P., Zhang, W.W., She, X.G., 2015. Concise total synthesis of (±)-aspidospermidine. Org. Biomol. Chem. 13, 5255–5259. https://doi.org/10.1039/c5ob00228a.

Mamatas-Kalamaras, S., Sévenet, T., Thal, C., Potier, P., 1975. Alcaloïdes d'*Alstonia quaternata*. Phytochemistry 14, 1849–1854. https://doi.org/10.1016/0031-9422(75)85309-X.

Maqbool, M., Mobashir, M., Hoda, N., 2016. Pivotal role of glycogen synthase kinase-3: a therapeutic target for Alzheimer's disease. Eur. J. Med. Chem. 107, 63–81. https://doi.org/10.1016/j.ejmech.2015.10.018.

Mark, P., Nilsson, L., 2001. Structure and dynamics of the TIP3P, SPC, and SPC/E water models at 298 K. J. Phys. Chem. 105, 9954–9960. https://doi.org/10.1021/jp003020w.

Martin, C.L., Nakamura, S., Otte, R., Overman, L.E., 2011. Total synthesis of (+)-condylocarpine, (+)-isocondylocarpine, and (+)-tubotaiwine. Org. Lett. 13, 138–141. https://doi.org/10.1021/ol102709s.

Martinez, A., Alonso, M., Castro, A., Perez, C., Moreno, F.J., 2002. First non-ATP competitive glycogen synthase kinase 3 beta (GSK-3beta) inhibitors: Thiadiazolidinones (TDZD) as potential drugs for the treatment of Alzheimer's disease. J. Med. Chem. 45, 1292–1299. https://doi.org/10.1021/jm011020u.

Mokrý, J., Dubravkova, L., Sefcovic, P., 1962. Alkaloids from Vinca minor L. Vincadine, minovine, and vincorine. Experientia 18, 564–565. https://doi.org/10.1007/BF02172182.

Mokrý, J., Kompiš, I., Shamma, M., Shine, R.J., 1964. Structure of vincaminorine and its relation to vincaminoreine and vincadine. Chem. Ind. 1988–1989.

Morris, G.M., Huey, R., Lindstrom, W., Sanner, M.F., Belew, R.K., Goodsell, D.S., Olson, A.J., 2009. AutoDock4 and AutoDockTools4: automated docking with selective receptor flexibility. J. Comput. Chem. 30, 2785–2791. https://doi.org/10.1002/jcc.21256.

Mroue, M.A., Euler, K.L., Ghuman, M.A., Alam, M., 1996. Indole alkaloids of *Haplophyton crooksii*. J. Nat. Prod. 59, 890–893. https://doi.org/10.1021/np960070c.

Nachon, F., Carletti, E., Ronco, C., Trovaslet, M., Nicolet, Y., Jean, L., Renard, P.Y., 2013. Crystal structures of human cholinesterases in complex with huprine W and tacrine: elements of specificity for anti-Alzheimer's drugs targeting acetyl- and butyryl-cholinesterase. Biochem. J. 453, 393–399. https://doi.org/10.1042/BJ20130013.

Naerum, L., Norskov-Lauritsen, L., Olesen, P.H., 2002. Scaffold hopping and optimization towards libraries of glycogen synthase kinase-3 inhibitors. Bioorg. Med. Chem. Lett. 12, 1525–1528. https://doi.org/10.1016/s0960-894x(02)00169-5.

O'Boyle, N.M., Banck, M., James, C.A., Morley, C., Vandermeersch, T., Hutchison, G.R., 2011. Open Babel: an open chemical toolbox. J. Cheminf. 3, 33. https://doi.org/10.1186/1758-2946-3-33.

Palmisano, G., Santagostino, M., Riva, S., Sisti, M., 1995. Indole alkaloids. Enantiocontrolled synthesis and absolute configuration of (+)-decarbomethoxy-15,20;16,17-tetrahydrosecodine. Tetrahedron Asymmetry 6, 1229–1232. https://doi.org/10.1016/0957-4166(95)00150-N.

Panek, D., Więckowska, A., Wichur, T., Bajda, M., Godyń, J., Jończyk, J., Mika, K., Janockova, J., Soukup, O., Knez, D., Korabecny, J., Gobec, S., Malawska, B., 2017. Design, synthesis and biological evaluation of new phthalimide and saccharin derivatives with alicyclic amines targeting cholinesterases, beta-secretase and amyloid beta aggregation. Eur. J. Med. Chem. 125, 676–695. https://doi.org/10.1016/j.ejmech.2016.09.078.

Pauptit, R.A., Trotter, J., 1981. Crystal structure of raucubaine. Can. J. Chem. 59, 1007–1009. https://doi.org/10.1139/v81-146.

Pettersen, E.F., Goddard, T.D., Huang, C.C., Couch, G.S., Greenblatt, D.M., Meng, E.C., Ferrin, T.E., 2004. UCSF Chimera–a visualization system for exploratory research and analysis. J. Comput. Chem. 25, 1605–1612. https://doi.org/10.1002/jcc.20084.

Plat, M., Men, J.L., Janot, M.M., Budzikiewicz, H., Wilson, J.M., Durham, L.J., Djerassi, C., 1962. Periwinkles alkaloids. XXVI. Application of mass spectrography to the determination of structure and stereochemistry. 17. Structure of four alkaloids of *Vinca minor*: (−)-vincadifformine, minovincine, minovincinine, and 16-methoxyminovincine. Bull. Soc. Chim. Fr. 2237–2241.

Polgar, L., 2002. The prolyl oligopeptidase family. Cell. Mol. Life Sci. 59, 349–362. https://doi.org/10.1007/s00018-002-8427-5.

Rayasam, G.V., Tulasi, V.K., Sodhi, R., Davis, J.A., Ray, A., 2009. Glycogen synthase kinase 3: more than a namesake. Br. J. Pharmacol. 156, 885–898. https://doi.org/10.1111/j.1476-5381.2008.00085.x.

Shi, B.-B., Chen, J., Bao, M.-F., Zeng, Y., Cai, X.-H., 2019. Alkaloids isolated from *Tabernaemontana bufalina* display xanthine oxidase inhibitory activity. Phytochemistry 166, 112060. https://doi.org/10.1016/j.phytochem.2019.112060.

Sierra, P., Novotny, L., Samek, Z., Budesinsky, M., Dolejs, L., Blaha, K., 1982. Alkaloids of *Rauvolfia salicifolia* GRISEB species. Collect. Czech. Chem. Commun. 47, 2912–2921. https://doi.org/10.1135/cccc19822912.

Singh, M., Kaur, M., Kukreja, H., Chugh, R., Silakari, O., Singh, D., 2013. Acetylcholinesterase inhibitors as Alzheimer therapy: from nerve toxins to neuroprotection. Eur. J. Med. Chem. 70, 165–188. https://doi.org/10.1016/j.ejmech.2013.09.050.

Soukup, O., Jun, D., Zdarova-Karasova, J., Patocka, J., Musilek, K., Korabecny, J., Krusek, J., Kaniakova, M., Sepsova, V., Mandikova, J., Trejtnar, F., Pohanka, M., Drtinova, L., Pavlik, M., Tobin, G., Kuca, K., 2013. A resurrection of 7-MEOTA: a comparison with tacrine. Curr. Alzheimer Res. 10, 893–906. https://doi.org/10.2174/1567205011310080011.

Stavrakov, G., Philipova, I., Zheleva-Dimitrova, D., Valkova, I., Salamanova, E., Konstantinov, S., Doytchinova, I., 2017. Docking-based design and synthesis of galantamine-camphane hybrids as inhibitors of acetylcholinesterase. Chem. Biol. Drug Des. 90, 709–718. https://doi.org/10.1111/cbdd.12991.

Tan, P.W., Seayad, J., Dixon, D.J., 2016. Expeditious and divergent total syntheses of Aspidosperma alkaloids exploiting Iridium(I)-Catalyzed generation of reactive Enamine intermediates. Angew Chem. Int. Ed. Engl. 55, 13436–13440. https://doi.org/10.1002/anie.201605503.

Tarrago, T., Kichik, N., Seguí, J., Giralt, E., 2007. The natural product berberine is a human prolyl oligopeptidase inhibitor. ChemMedChem 2, 354–359. https://doi.org/10.1002/cmdc.200600303.

Trott, O., Olson, A.J., 2010. AutoDock Vina: improving the speed and accuracy of docking with a new scoring function, efficient optimization, and multithreading. J. Comput. Chem. 31, 455–461. https://doi.org/10.1002/jcc.21334.

Ur-Rahman, A., Abbas, S.A., Nighat, F., Ahmed, G., Choudhary, M.I., Alvi, K.A., Ur-Rehman, H., de Silva, K.T.D., Arambewela, L.S.R., 1991a. Chemical constituents of *Alstonia macrophylla*. J. Nat. Prod. 54, 750–754. https://doi.org/10.1021/np50075a002.

Ur-Rahman, A., Zaman, K., Perveen, S., Ur-Rehman, H., Muzaffar, A., Choudhary, M.I., Pervin, A., 1991b. Alkaloids from *Rhazya stricta*. Phytochemistry 30, 1285–1293. https://doi.org/10.1016/S0031-9422(00)95218-X.

Varga, S., Angyal, P., Martin, G., Egyed, O., Holczbauer, T., Soós, T., 2020. Total syntheses of (−)-Minovincine and (−)-Aspidofractinine through a sequence of cascade reactions. Angew Chem. Int. Ed. Engl. 59, 13547–13551. https://doi.org/10.1002/anie.202004769.

Vas, A., Gulyas, B., 2005. Eburnamine derivatives and the brain. Med. Res. Rev. 25, 737–757. https://doi.org/10.1002/med.20043.

Wang, J., Wolf, R.M., Caldwell, J.W., Kollman, P.A., Case, D.A., 2004. Development and testing of a general amber force field. J. Comput. Chem. 25, 1157–1174. https://doi.org/10.1002/jcc.20035.

Wang, J., Wang, W., Kollman, P.A., Case, D.A., 2006. Automatic atom type and bond type perception in molecular mechanical calculations. J. Mol. Graph. Model. 25, 247–260. https://doi.org/10.1016/j.jmgm.2005.12.005.

Wenkert, E., Liu, S., 1994. Total synthesis of (±)-Aspidofractinine and (±)-Aspidospermidine. J. Org. Chem. 59, 7677–7682. https://doi.org/10.1021/jo00104a023.

WHO, 2020. Dementia. https://www.who.int/news-room/fact-sheets/detail/dementia. (Accessed 27 August 2021). accessed.

Williams, D., Qu, Y., Simionescu, R., de Luca, V., 2019. The assembly of (+)-vincadifformine- and (−)-tabersonine-derived monoterpenoid indole alkaloids in *Catharanthus roseus* involves separate branch pathways. Plant J. 99, 626–636. https://doi.org/10.1111/tpj.14346.

Wong, S.-K., Yeap, J.S.-Y., Tan, C.-H., Sim, K.-S., Lim, S.-H., Low, Y.-Y., Kam, T.-S., 2021. Arbolodinines A-C, biologically-active aspidofractinine-aspidofractinine, aspidofractinine-strychnan, and kopsine-strychnan bisindole alkaloids from *Kopsia arborea*. Tetrahedron 78, 131802. https://doi.org/10.1016/j.tet.2020.131802.

Wright, C.I., Geula, C., Mesulam, M.M., 1993. Neuroglial cholinesterases in the normal brain and in Alzheimer's disease: relationship to plaques, tangles, and patterns of

selective vulnerability. Ann. Neurol. 34, 373–384. https://doi.org/10.1002/ana.410340312.

Xu, H., Huang, H., Zhao, C., Song, C., Chang, J., 2019. Total synthesis of (+)-Aspidospermidine. Org. Lett. 21, 6457–6460. https://doi.org/10.1021/acs.orglett.9b02346.

Yagudaev, M.R., 1984. The NMR study of alkaloids. VI. A comparison of the stereochemistries of pseudocopsinine and 14,15-dihydrovindolinine by ^{13}C NMR spectroscopy. Chem. Nat. Compd. 20, 311–314. https://doi.org/10.1007/BF00575755.

Yuan, Z.Q., Ishikawa, H., Boger, D.L., 2005. Total synthesis of natural (−)- and ent-(+)-4-Desacetoxy-6,7-dihydrovindorosine and natural and ent-minovine:oxadiazole Tandem intramolecular Diels−Alder/1,3-DipolarCycloaddition reaction. Org. Lett. 7, 741–744. https://doi.org/10.1021/ol0507423.

Zachystalová, D., Strouf, O., Trojanek, J., 1963. New alkaloids of *Vinca minor*. Chem. Ind. 610–611.

Zeng, X., Shukla, V., Boger, D.L., 2020. Divergent total syntheses of (−)-Pseudocopsinine and (−)-Minovincinine. J. Org. Chem. 85, 14817–14826. https://doi.org/10.1021/acs.joc.0c02493.

Zenk, M.H., Juenger, M., 2007. Evolution and current status of the phytochemistry of nitrogenous compounds. Phytochemistry 68, 2757–2772. https://doi.org/10.1016/j.phytochem.2007.07.009.